Additive Manufacturing in Ka-band Antenna Engineering

Alec Robin Gould
Department of Electrical and Smart Systems Engineering
College of Science, Engineering and Technology
University of South Africa
Florida, Johannesburg, South Africa
Email: argould2277@gmail.com

Prof. Sumbwanyambe Mbuyu
Department of Electrical and Smart Systems Engineering
College of Science, Engineering and Technology
University of South Africa
Florida, Johannesburg, South Africa
Email: sumbwm@unisa.ac.za

Dr. Khumbelo Difference Muthavhine
Department of Electrical and Smart Systems Engineering
College of Science, Engineering and Technology
University of South Africa
Florida, Johannesburg, South Africa
Email: kdmuthavhine@gmail.com

Abstract— **This research aims to evaluate the design, manufacturing, and optimization of a ka-band pyramidal horn antenna using advanced additive manufacturing. Traditional manufacturing methods for high-frequency antennas face limitations in geometries and material usage. This study explores the potential of three-dimensional (3D) printing, particularly Stereolithography (SLA), to overcome these challenges. By integrating palladium-free electroless plating techniques, the conductive properties necessary for effective antenna performance are achieved. The research employs both computational simulations using Python and Ansys HFSS, and physical experiments to validate the antenna's performance. The results are expected to demonstrate close to equivalence in electromagnetic performance, reduced material waste and cost, and enhanced design flexibility, contributing to the advancement of antenna technology in high-frequency applications.**

Keywords—Antenna, additive manufacturing, SLA 3D printing, ka-band, electromagnetics, telecommunication, microwave, millimeter wave, electroless plating

I. INTRODUCTION

Traditionally, horns have been manufactured using "conventional" techniques such as milling, turning, or casting, which often pose limitations in terms of design complexity, production time, and cost. However, with the advent of additive manufacturing (AM) techniques, new possibilities have emerged for enhancing the design, manufacturing, and implementation processes of antennas [1]. See Fig. 1 for an example of an AM antenna used in this paper.

AM, offers the flexibility to fabricate intricate geometries with high precision, opening doors to novel antenna designs that were previously unattainable. By leveraging AM, researchers can explore innovative horn antenna configurations tailored for specific applications, optimizing parameters such as gain, directivity, and bandwidth [2]. Moreover, the use of AM in antenna production holds promise for streamlining manufacturing processes, reducing material waste, saving weight, and ultimately lowering production costs. These advantages not only make antennas more accessible to researchers and engineers but also pave the way for custom-tailored antennas optimized for individual requirements.

In recent years, the ka-band frequency range (26.5 - 40 GHz) has gained prominence in various applications, including satellite communications, radar systems, and remote sensing. The demand for high-performance antennas operating in this frequency band has spurred interest in developing antennas optimized specifically for ka-band applications [3]. As the signal frequency goes up, the wavelength becomes smaller, hence, the antenna's physical size becomes smaller, and tolerances become less forgiving.

This study aims to explore the design, manufacturing, and implementation of a ka-band PHA using additive manufacturing techniques. By harnessing the capabilities of AM, the goal is to achieve enhanced performance characteristics, including improved gain and directivity, tailored to the unique requirements of ka-band applications. Through rigorous experimentation and analysis, this research seeks to contribute to the advancement of antenna technology in the ka-band frequency range, opening possibilities for more novel and complex high-frequency research.
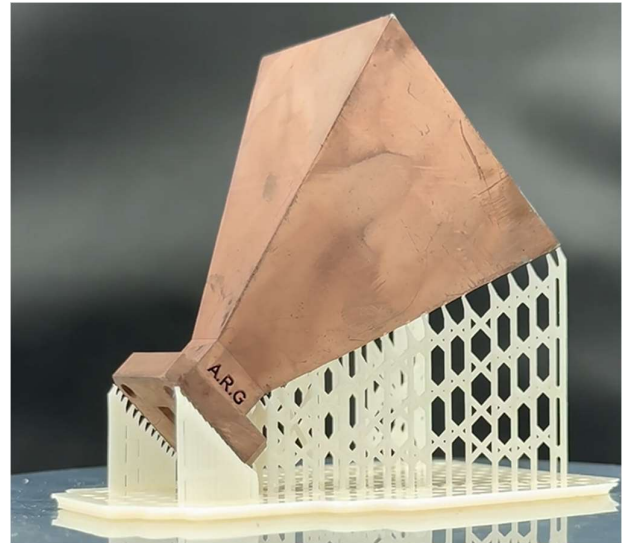

Fig. 1: Additively manufactured horn antenna perched upon it's 3D printed support structure

The theoretical backgrounds of pyramidal horn antennas and the additive manufacturing process' are given in Section II of this paper. In Section III the pyramidal horn antennas used for research are designed. In Section IV the developed AM technique is presented. The 3D printed, metal-plated horn antennas' measured results are evaluated in Section V ,and the paper concluded in Section VI.

II. THEORETICAL BACKGROUND

A. Pyramidal Horn Antennas

The horn antenna is, fundamentally, a transition from the waveguide impedance to free-space impedance using the gradual flaring of the waveguide to selectively radiate power in a given direction. The shape of the flare, length and angle of the taper can have a significant effect on the electromagnetic properties [4], [5]. Pyramidal horn antennas serve as fundamental components in the field of antenna engineering, facilitating the transition from a coaxial cable to waveguide to antenna topology. Their simple yet effective design enables stable radiation patterns and consistent gain across a wide frequency range [4].

The analysis begins with the approximation of the tangential components of the E- and H-fields over the aperture of the horn antenna. These components are given by [4], [5]:

$$E_y'(x', y') = E_0 \cos\left(\frac{\pi x'}{A}\right) e^{-j\left[\frac{k(x'^2/R_2 + y'^2/R_1)}{2}\right]} \quad (1)$$

$$H_x'(x', y') = -\frac{E_0}{\eta} \cos\left(\frac{\pi x'}{a_1}\right) e^{-j\left[\frac{k(x'^2/R_2 + y'^2/R_1)}{2}\right]} \quad (2)$$

x', and y' are the unit vectors (See Fig. 2). The equivalent current densities are then defined as [4], [5]:

$$J_y(x', y') = -\frac{E_0}{\eta} \cos\left(\frac{\pi x'}{A}\right) e^{-j\left[\frac{k\left(\frac{x'^2}{R_2} + \frac{y'^2}{R_1}\right)}{2}\right]} \quad (3)$$

$$M_x(x', y') = E_0 \cos\left(\frac{\pi x'}{A}\right) e^{-j\left[\frac{k\left(\frac{x'^2}{R_2} + \frac{y'^2}{R_1}\right)}{2}\right]} \quad (4)$$

The far-zone E- and H-field components can be derived from the equivalent current densities, leading to the following expressions for the radiated fields [4], [5]:

$$E_r = 0 \quad (5)$$

$$E_\theta = -j\frac{kE_0 e^{-jkr}}{4\pi r} \sin\phi (1 + \cos\theta) I_1 I_2 \quad (6)$$

$$E_\phi = -j\frac{kE_0 e^{-jkr}}{4\pi r} \cos\phi (\cos\theta + 1) I_1 I_2 \quad (7)$$

Where I_1 and I_2 are given by [4], [5]

$$I_1 = \int_{-\frac{A}{2}}^{\frac{A}{2}} \cos\left(\frac{\pi}{a} x'\right) e^{-jk\left[\frac{x'^2}{2R_1} - x' \sin(\theta)\cos(\phi)\right]} dx' \quad (8)$$

$$I_2 = \int_{-\frac{B}{2}}^{\frac{B}{2}} e^{-jk\left[\frac{y'^2}{2R_1} - y' \sin(\phi)\sin(\theta)\right]} dx' \quad (9)$$
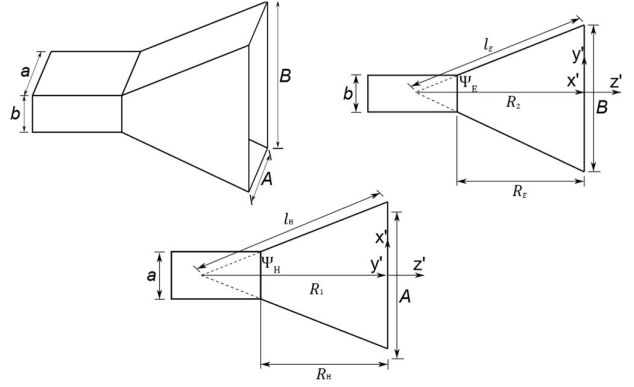

Fig. 2: Fully annotated diagram of a pyramidal horn antenna.

1) Traditional Horn Design Technique

a) Step 1

Specify the following parameters:

- sought after gain (G_0) as a ratio and not in dB
- centre frequency of operation (f) in hertz
- waveguide dimensions (a and b in meters

b) Step 2

Solve for χ using (10) until χ satisfies (11) and (12). Obtaining χ_{trial} is an iterative process:

$$\chi_{trial} = \chi_1 = \frac{G_0}{2\pi\sqrt{2\pi}} \quad (10)$$

$$l_E = \chi\lambda \quad (11)$$

$$l_H = \frac{G_0^2}{8\pi^3}\left(\frac{1}{\chi}\right)\lambda \quad (12)$$

The verification of whether χ satisfies (11) and (12), can be done using (14).

$$G_0 \approx \frac{2\pi}{\lambda^2} \sqrt{3\lambda l_H}\sqrt{2\lambda l_E} \quad (13)$$

c) Step 3

This step entails back calculating the remainder of the parameters. Narrow, and broad sides of the horn flare can be calculated using χ:

$$A = \frac{G_0}{2\pi}\sqrt{\frac{3}{2\pi\chi}}\lambda \quad (14)$$

$$B = \sqrt{2\chi}\lambda \quad (15)$$

The lengths of the horn flare can be calculated using (16) and (17):

$$R_E = (B - b)\left[\left(\frac{l_E}{B}\right) - \frac{1}{4}\right]^{\frac{1}{2}} \quad (16)$$

$$R_H = (A - a)\left[\left(\frac{l_h}{A}\right) - \frac{1}{4}\right]^{\frac{1}{2}} \quad (17)$$

2) Optimum Horn Design Technique
   a) Step 1
Specify the following parameters:

- sought after gain (G) as a ratio and not in dB

- centre frequency of operation (f) in hertz

- waveguide dimensions (a and b) in meters

   b) Step 2
Solve the roots of the following fourth-order quadratic equation:

$$A^4 - aA^3 + \frac{3bG\lambda^2}{8\pi\varepsilon_{ap}}A - \frac{3G^2\lambda^4}{32\pi^2\varepsilon_{ap}^2} = 0 \qquad (18)$$

Where:

$$\varepsilon_{ap} = 0.51 \qquad (19)$$

$$\lambda = \frac{c}{f} = \frac{2.9979 \times 10^8}{f} \; meters \qquad (20)$$

Whose coefficients are in the form:

$$fx^4 + gx^3 + hx^2 + ix + j = 0 \qquad (21)$$

$$\begin{aligned} f &= 1 \\ g &= -a \\ h &= 0 \\ i &= \frac{3bG\lambda^2}{8\pi\varepsilon_{ap}} \\ j &= \frac{3G^2\lambda^4}{32\pi^2\varepsilon_{ap}^2} \end{aligned} \qquad (22)$$

   The roots of this equation will yield the dimension of broad side of the flare of the horn (A) in meters. Take note that negative roots, or any roots containing imaginary components can be discarded.

   c) Step 3
   This step entails back calculating the remainder of the parameters. Obtain B, the narrow side of the flare of the horn, by back calculating using the gain equation:

$$G = 0.51\frac{4\pi}{\lambda^2}AB$$

$$B = \frac{G}{0.51\frac{4\pi}{\lambda^2}A} \qquad (23)$$

Obtain R_1, R_H and l_H:

$$A = \sqrt{3\lambda R_1}$$
$$R_1 = \frac{A^2}{3\lambda} \qquad (24)$$

$$\frac{R_1}{R_H} = \frac{A}{A-a}$$
$$R_H = \frac{A-a}{A}R_1 \qquad (25)$$

$$l_H{}^2 = R_1{}^2 + \left(\frac{A}{2}\right)^2$$
$$l_H = \sqrt{R_1{}^2 + \left(\frac{A}{2}\right)^2} \qquad (26)$$

Obtain R_2, R_E and l_E::

$$B = \sqrt{2\lambda R_2}$$
$$R_2 = \frac{B^2}{2\lambda} \qquad (27)$$

$$\frac{R_2}{R_E} = \frac{B}{B-b}$$
$$R_E = \frac{B-b}{B}R_2 \qquad (28)$$

$$l_E{}^2 = R_2{}^2 + \left(\frac{B}{2}\right)^2$$
$$l_E = \sqrt{R_2{}^2 + \left(\frac{B}{2}\right)^2} \qquad (29)$$

   d) Step 4
Validate your solution by checking:

$$R_E = R_H \qquad (30)$$

$$s = \frac{1}{8}\left(\frac{B}{\lambda}\right)^2\frac{\lambda}{R_2} = 0.25 \qquad (31)$$

$$t = \frac{1}{8}\left(\frac{A}{\lambda}\right)^2\frac{\lambda}{R_1} = 0.375 \qquad (32)$$

   If this step checks out ($s = 0.25$ and $t = 0.375$), the calculated geometries may be considered mathematically sound.

3) Tuned Horn Design
   This variant of the pyramidal horn employs the traditional horn design technique, but had it's geometries ($A, B, R_E = R_H$) optimised using Ansys HFSS optimetrics (Adaptive single objective with a goal of 20 dB gain). Fig. 3 shows the horn model used to simulate all three variants.
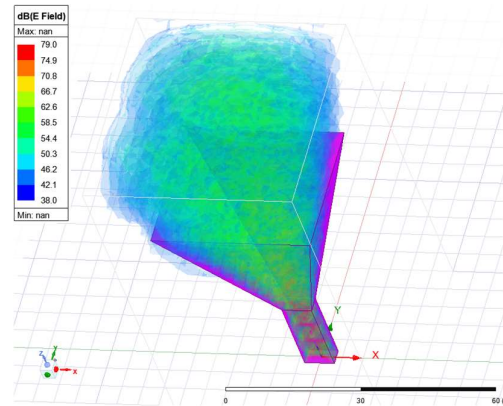

Fig. 3: Simulated pyramidal horn antenna model in Ansys HFSS.

III. PYRAMIDAL HORN DESIGN

The following specifications are given for the horn:

- Gain: 20 dB
- Band: 26.5 – 40 GHz
- Interface: WR28

Using the techniques from Section II, Table 1 is generated and the important dimensions are given.

Table 1: Generated pyramidal horn antenna dimensions.

Variant	Flare width (A)	Flare height (B)	Flare length ($R_E = R_H$)
Traditional	40.285 mm	31.429 mm	46.501 mm
Optimum	40.165 mm	31.581 mm	49.081 mm
Tuned	38.000 mm	31.861 mm	42.829 mm

The horns from Table 1 were simulated in Ansys HFSS, Table 2 shows the general expected results. Comparing both tables, it is clear that a fairly significant change in Flare length, width, or height does not significantly affect reflection coefficient or gain.

Table 2: Expected performance of the horn antennas

Variant	Reflection coefficient (S_{11})	Boresight gain (G)
Traditional	-27.31 dB	20.53 dB
Optimum	-27.40 dB	20.72 dB
Tuned	-27.38 dB	20.21 dB

Autodesk Fusion 360 is used to model the antennas, as seen in Fig. 4, using real world considerations, such as wall thickness, mechanical interfaces, antenna identification debossing, etc.
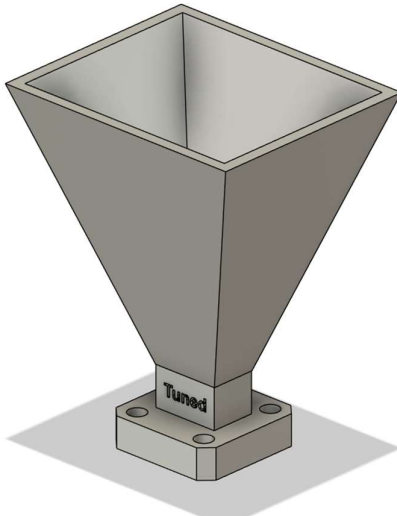

Fig. 4: 3D model designed from the simulated horn model.

IV. ADDITIVE MANUFACTURING

A. 3D printing

The manufacturing files were generated by Chitubox, configured to 3D print with a Creality Halot Mage 3D printer using SunLu high-temperature resin. The design of the manufacturing files follows two main paths: precision and minimal post-processing. This can be considered a critical step in this research project, since unsought after variations in physical dimensions or an irregular WR28 flange will limit the potential of this research. There is a difficult balance between ensuring the part receives enough support material, but also maintaining minimal post-processing. This was an iterative process, but ultimately the "perfect" balance was obtained by rotating the part 45 degrees, and inserting support material only where completely necessary and not on any electromagnetic paths. Fig. 5 and Fig. 6 shows the support material mounting at the side of the WR28 flange.

Fig. 5: SLA 3D printed horn side view support structure.

One can expect around 1 voxel (three-dimensional pixel) worth of accuracy for printed parts, which in this case is 25x25x10 micron.

Fig. 6: SLA 3D printed horn rear view support structure.

B. Electroless plating

The electroless plating method utilised in this research combines a few pre-existing techniques, modified to fit this application [6], [7], [8], [9], [10], [11], [12], [13]. An orthogonal experimental matrix was designed to obtain specific quantities of chemicals, correct operating conditions, and processes.

1) Surface preparation

This step consists of a thorough degreasing, and a careful etching. Isopropanol is used to clean the part, sodium hydroxide is used as a degreaser, and an etchant [14]. This removes the need to use the typical chromium trioxide.

2) Neutralisation 1

This step is used as a transition between very alkali conditions in the etching, to the acidic conditions in the sensitisation. A dilute solution of hydrochloric acid neutralises the part. The part is then washed in deionised water.

3) Sensitisation

stannous chloride is used as the sensitizer, to allow tin to be adsorbed onto the surface of the etched part. The part is then washed in deionised water.

4) Neutralisation 2

This step is used as a transition between acidic conditions in the sensitisation, to the alkali conditions in the activation. A dilute solution of ammonium hydroxide and sodium carbonate neutralises the part. The part is then washed in deionised water.

5) Activation

Silver nitrate is used as the activator – a catalytic surface deposition. A more stable activator solution was developed using ammonium hydroxide to form a complex with the silver – borrowed from the Tollen Reagent [15].

6) Plating

The chosen metal plating is copper. As a result the plating bath consists of a modified version from [6], [7], and [11]:

- copper sulphate pentahydrate ($CuSO_4 \cdot 5H_2O$)
- tetrasodium ethylenediaminetetraacetic acid ($Na_4EDTA \cdot 4H_2O$)
- sodium hydroxide (NaOH)
- formaldehyde (CH_2O)
- various additives for grain refinement, reaction rate control. Such as thiourea and polyethylene glycol (PEG)

Test strips are used to evaluate the efficacy of electroless plating. Fig. 7 Shows the copper-coated resin-printed test strip. A simple fingernail scratch test is performed to determine whether the copper layer is sufficiently adhered. Fig. 1 displays a pyramidal horn antenna, that utilised the above method to copper plate it.

Fig. 7: Copper plated SLA 3D printed test strip. Front view (Left image) and rear view (Right image).

V. RESULTS

In total six antennas were manufactured and evaluated. Reflection coefficient measurements were performed as shown in Fig. 8. Two Quinstar QWA-28S24F coax to waveguide adapters were used. The measurements were performed using an Agilent 8510C vector network analyser, calibrated up to the end of the coax cable – not including the coax to waveguide. Mean reflection coefficient results are recorded in Table 3. The "optimum" variant was excluded from here as this antenna was about 10% physically larger for no performance benefit.

Fig. 9 and Fig. 10 show the comparison of the manufactured antennas vs the simulated. There is an obvious hit in performance, this is likely due to the coax-to-waveguide (VSWR of 1.25) and the mismatch at the WR-28 coupling. The variance between measured results shows that the additive manufacturing process used here can be improved upon to achieve consistency comparable to traditionally manufactured antennas. Gain, and radiation pattern measurements would add valuable insight to this study and should be considered for the future.
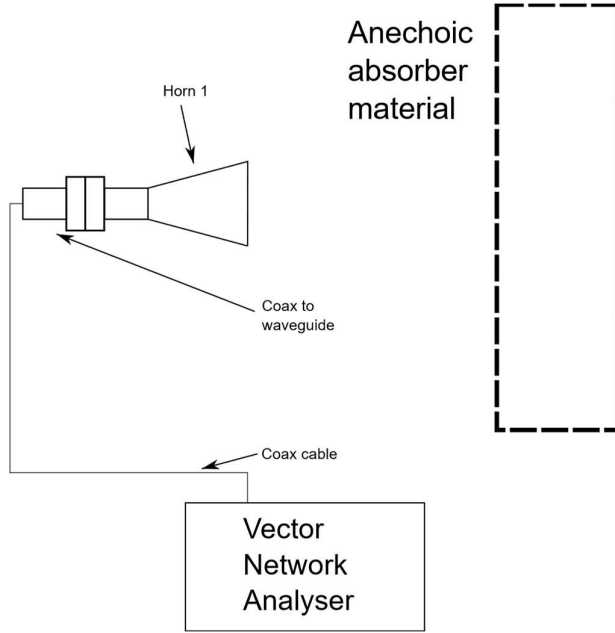
Fig. 8: Measurement setup for the evaluation of reflection coefficient.

Table 3: Additively manufactured horn antenna measured reflection coefficient(mean) results.

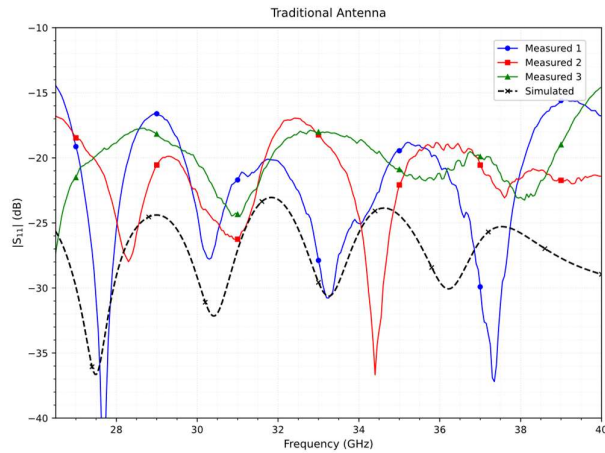| Variant	Reflection coefficient (S_{11})
Traditional 1	-22.25 dB
Traditional 2	-21.66 dB
Traditional 3	-20.08 dB
Tuned 1	-22.68 dB
Tuned 2	-24.01 dB
Tuned 3	-22.89 dB

Fig. 9: Measured vs simulated reflection coefficient results for the traditionally designed horn antenna.
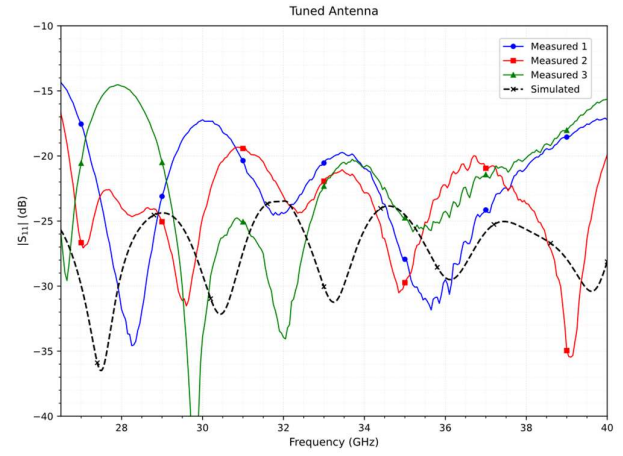

Fig. 10: Measured vs simulated reflection coefficient results for the HFSS tuned horn antenna.

VI. CONCLUSION

Six ka-band pyramidal horn antennas were designed, 3D printed, and copper-plated using a palladium-free electroless process. Measurements show agreement with simulations, confirming that additive manufacturing can deliver high-frequency antennas with performance potentially comparable to conventional methods. The approach offers reduced cost, material savings, and greater design flexibility, making it a promising technique for future millimetre-wave research.

REFERENCES

[1] Y. Wang *et al.*, "3D Printed Antennas for 5G Communication: Current Progress and Future Challenges," *Chinese Journal of Mechanical Engineering: Additive Manufacturing Frontiers*, vol. 2, no. 1, p. 100065, Mar. 2023, doi: 10.1016/j.cjmeam.2023.100065.

[2] K. Lomakin, J. Schür, and G. Gold, "Design Optimization of Pyramidal Horn Antennas for 3D Printing in the mm-Wave Range."

[3] A. Alam, S. Urooj, and A. Q. Ansari, "Design and Simulation of 24 GHz high gain pyramidal Horn Antenna for Bio-Radar Sensing Application," in *2023 International Conference on Recent Advances in Electrical, Electronics and Digital Healthcare Technologies, REEDCON 2023*, Institute of Electrical and Electronics Engineers Inc., 2023, pp. 596–599. doi: 10.1109/REEDCON57544.2023.10151440.

[4] C. A. Balanis, *Antenna Theory Analysis and Design*, 4th ed. Wiley, 2016.

[5] D. M. Pozar, *Microwave engineering*, 4th ed. Wiley, 2012.

[6] Cheryl A. Deckert, "Electroless Copper Plating, a review," *Plating & Surface finishing*, pp. 48–55, Feb. 1995.

[7]   G. O. Mallory and J. B. Hajdu, *Electroless Plating: Fundamentals And Applications*. American Electroplaters and Surface Finishers Society, 1990.

[8]   S. Swee Song, "Development of a Novel Method In Electroless Copper Plating," 2004.

[9]   S. Shukla, S. Seal, Z. Rahaman, and K. Scammon, "Electroless copper coating of cenospheres using silver nitrate activator." [Online]. Available: www.elsevier.com/locate/matlet

[10]   R. Bernasconi, C. Credi, M. Tironi, M. Levi, and L. Magagnin, "Electroless Metallization of Stereolithographic Photocurable Resins for 3D Printing of Functional Microdevices," *J Electrochem Soc*, vol. 164, no. 5, pp. B3059–B3066, 2017, doi: 10.1149/2.0081705jes.

[11]   A. Kaewvilai, R. Tanathakorn, A. Laobuthee, W. Rattanasakulthong, and A. Rodchanarowan, "Electroless copper plating on nano-silver activated glass substrate: A single-step activation," *Surf Coat Technol*, vol. 319, pp. 260–266, Jun. 2017, doi: 10.1016/j.surfcoat.2017.04.018.

[12]   L. M. Luo *et al.*, "Electroless copper plating on PC engineering plastic with a novel palladium-free surface activation process," *Surf Coat Technol*, vol. 251, pp. 69–73, Jul. 2014, doi: 10.1016/j.surfcoat.2014.04.005.

[13]   Z. Jing, "Development of Electroless Plating Processes for Low Cost Plastic-Metallization and Area-Selective Metal Coating of Three-Dimensional Structures," 2020.

[14]   M. Schneider *et al.*, "Surface etching of 3D printed poly(lactic acid) with NaOH: A systematic approach," *Polymers (Basel)*, vol. 12, no. 8, Aug. 2020, doi: 10.3390/POLYM12081711.

[15]   W. E. Benet, G. S. Lewis, L. Z. Yang, and D. E. Peter Hughes, "The mechanism of the reaction of the Tollens reagent," *J Chem Res*, vol. 35, no. 12, pp. 675–677, Dec. 2011, doi: 10.3184/174751911X13206824040536.